Transition from nonlocal electron transport to radiative regime in an expanding blast wave

Marocchino, A., Ravasio, A., Levy, A., Lancia, L., Fukuda, Y., Jinno, S., Atzeni, S., Doria, D., Prigent, C., Lamour, E., Vernhet, D., Borghesi, M., & Romagnani, L. (2018). Transition from nonlocal electron transport to radiative regime in an expanding blast wave. *Applied Physics Letters*, *112*(26), 1-6. Article 264104. https://doi.org/10.1063/1.5022698

Published in:
Applied Physics Letters

Document Version:
Peer reviewed version

This manuscript was accepted by Appl. Phys. Lett. Click here to see the version of record.

Transition from Nonlocal Electron Transport to Radiative Regime in an expanding blast wave

A. Marocchino,[1,2] A. Ravasio,[3] A. Levy,[4] L. Lancia,[3,2] Y. Fukuda,[5] S. Jinno,[6] S. Atzeni,[2] D. Doria,[7] C. Prigent,[8] E. Lamour,[8] D. Vernhet,[8] M. Borghesi,[7] and L. Romagnani[3]

[1)] *Istituto Nazionale di Fisica Nucleare, LNF, 00044 Frascati, Italy*
[2)] *Dipartimento SBAI, Università di Roma "La Sapienza", 00161 Rome, Italy*
[3)] *LULI, Ecole Polytechnique, CNRS, CEA, UPMC, Route de Saclay, 91128 Palaiseau, France*
[4)] *Institut des NanoSciences de Paris, Sorbonne Universités, UPMC Univ Paris 06, CNRS-UMR 7588, 75005, Paris, France*
[5)] *Kansai Photon Science Institute (KPSI), National Institutes for Quantum and Radiological Science and Technology (QST), 8-1-7 Umemidai, Kizugawa, Kyoto 619-0215, Japan*
[6)] *Nuclear Professional School, The University of Tokyo, 2-22 Shirakata Shirane, Tokai, Naka, Ibaraki 319-1188, Japan*
[7)] *School of Mathematics and Physics, The Queen's University of Belfast, Belfast BT7 1NN, UK*
[8)] *Sorbonne Université, CNRS-UMR 7588, Institut des NanoSciences de Paris -INSP, 75252, Paris Cedex 05, France*

(Dated: 14 June 2018)

We have investigated formation, evolution and late-time propagation of a laser-generated cylindrical blast wave. The whole blast wave evolution over timescales of several nanoseconds was reconstructed experimentally (via temporally-resolved interferometric measurements) and via hydrodynamic simulations that included modeling of nonlocal electron transport and radiation diffusion. Comparison between the experimental results and the simulations indicates that the early expansion phase is characterised by nonlocal electron heat transport causing energy spread on times shorter than the typical timescales for hydrodynamic expansion. Nonlocal electron transport ionizes the gas ahead of the plasma front and gives rise to a smooth radial density gradient. At later times, once the shock is launched and the BW is formed, radiation results in reduced shock velocity compared to the adiabatic case. These investigations provide a suitable and effective platform to benchmark the inclusion of kinetic and radiative effects in fluid modeling of the plasma dynamics over timescales that may be unaccessible to fully kinetic simulations.

We present a detailed investigation of laser-driven blast waves (BWs), which offer a chance to study high Mach number shock waves in the laboratory. In particular, we study the effects of nonlocal electron transport and radiation diffusion on BWs evolution. These fundamental properties are relevant to plasma applications, such as Inertial Confinement Fusion[1–3] and astrophysics[4–8]. BWs have been studied both theoretically[9,10] and experimentally. Experiments have shed light on a variety of aspects, including radiative dynamics and radiative properties[11–14], formation of secondary shocks at late-times[15], self-induction of magnetic fields[5], effects of nonlocal heat conduction at early evolution times[16], thermal plasma instabilities[17]. Collisions between two BWs have also been investigated[18]. In this letter, we report on the early effects played by nonlocal heat transport in BW formation and launching, when fast, free-streaming particles cause an energy spread on times shorter than the typical timescales for hydrodynamic expansion. Nonlocal heat conduction ionizes the gas ahead of the plasma front giving rise to a smooth density profile. At later times, once the BW is formed, radiation results in reduced shock velocity compared to the adiabatic case[19,20].

Gave their broad relevance in various contexts, electron and radiation transport mechanisms have been extensively investigated for laboratory astrophysics scenarios or in relation to ICF problems. Modelling nonlocal heat transport is however a non-trivial task, and a number of different approaches[21–26] have been developed. Electron heat transport is in fact a kinetic process intrinsically related to the deformations of the electron energy distribution function. According to the classical treatment of thermal conduction, based on first-order perturbation theory applied to the Fokker-Planck equation, the thermal flux is given by $Q_{\rm SH} = -\kappa_{\rm SH}\nabla T_{\rm e}$ with $\kappa_{\rm SH}$ the Spitzer-Härm (SH)[27] electron conductivity and $T_{\rm e}$ the electron temperature. However, it has been shown that as soon as the electron mean-free-path (mfp) exceeds about 2×10^{-3} times the temperature gradient scale-length, this expression breaks down[28], and long-range electron corrections need to be taken into account[21]. In the investigated case, the electron mfp $\lambda_{{\rm e},\,\pi/2} = T_e^2/4\pi ne^4(Z\Lambda_{ei} + \Lambda_{ee})$ (with n the electron number density, e the fundamental charge, Z the ion charge and Λ the Coulomb logarithms) becomes as large as the density gradient scale-length at the boundary of the laser-heated region. While a kinetic treatment is in principle required, performing fully kinetic simulations on hydrodynamic timescales may be computationally challenging. It is therefore necessary to rely on a fluid or *weakly-kinetic* approach, where suitable schemes to treat electron thermal transport must be implemented. In the simplest approach the limitation of thermal conductivity due to nonlocal effects is mocked-up by introduc-

This manuscript was accepted by Appl. Phys. Lett. Click here to see the version of record.

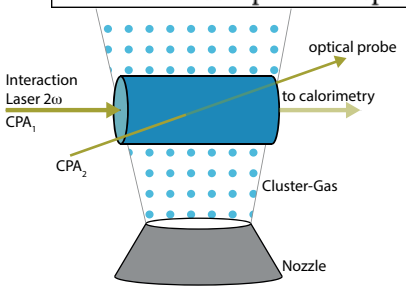

FIG. 1. Schematic experimental setup.

ing a flux-limitation to the SH model, $Q_f \leq f n v_t k_B T_e$, where v_t is the electron thermal velocity and f is the flux-limiter. More accurate treatments replace the heat diffusion kernel with a harmonic series truncated to first order, modeled as an energy dependent convolution operator $Q = Q_{SH} * w(\lambda_{e,g})$[21,22] (where $*$ is the convolution operator and w an appropriate weight, function of the mfp $\lambda_{e,g}$ of the electrons with energy E_g). Due to the complex interplay between transport and hydrodynamics, it is critical to validate such schemes against experimental investigations where the contribution of the different processes at play can be isolated.

In this Letter, we present the comparison between experimental observations and hydrodynamic simulations for the whole evolution of a laser-generated cylindrical BW. The different stages of the evolution are characterized by different scale-lengths[29]. Leveraging on a recent implementation of a nonlocal heat transport model for hydrodynamic timescales[30], we aim to identify the relevant underlying mechanisms throughout the whole evolution. The advantage to use BWs is twofold. First, the simple experimental setup allows comfortable diagnostics access. Second, self-similar models predict that BW radius R evolves in time as $R \propto t^{\alpha}$, where α depends on the physical processes at play (e.g. $\alpha = 1/2$ for the adiabatic case[7,20] and $\alpha = 1/3$ for the pressure driven snowplough[7]). Comparison of experimental data with such solutions allows to distinguish among the different evolution phases.

The experiment was performed at the Laboratoire d'Utilisation des Lasers Intenses (LULI) employing the ELFIE laser system, operating in the Chirped Pulse Amplification (CPA) mode. The experimental setup is depicted in Fig.1. A plasma filament was created in the interaction of a short and intense laser pulse with an Argon cluster-jet. The use of a cluster-jet ensured efficient absorption of the laser energy[31]. The short pulse duration ($\tau_L \sim 1$ ps) and tight focusing of the laser beam give a laser intensity $I_L \gtrsim 10^{18}$ W cm^{-2}, providing fast and localized energy deposition into the target. To prevent early disassembly of the clusters due to laser pulse pre-pulse, the pulse contrast was enhanced via frequency doubling, the laser wavelength and energy after conversion being $\lambda_L \simeq 0.53$ μm and $E_L \sim 3$ J, respectively. The laser was focused 2 mm from the gas nozzle where the density was approximately $\sim 10^{18}$ cm^{-3}, known from independent characterization. The laser energy was deposited over a length of 3 mm, and the fraction of laser energy transmitted through the cluster-jet was measured via absolutely calibrated calorimetry, yielding estimations for the maximum absorption efficiencies of $\sim 70\%$. The plasma generated in the interaction of the laser pulse with the cluster-jet was characterized via optical imaging interferometry in a modified Nomarski arrangement. A multi-mJ (~ 100 mJ), frequency-doubled (wavelength ~ 0.53 μm) auxiliary laser pulse (CPA_2) was used as optical probe. Interferometry measurements provided a spatially and temporally resolved mapping of the plasma electron density.

The temporal evolution of the plasma spanning for tens of nanoseconds was reconstructed by varying the relative delay of the CPA_2 probe with respect to CPA_1. Typical examples of the interferograms with Abel-inverted electron density radial profiles are shown in Fig. 2 (additional time frames are shown in Fig. 3). The Abel-inverted density profiles indicate that, within the error bar associated with the deconvolution process, at the earliest probing times (t 0.03 ns) a plasma filament is created with relatively smooth radial gradients and long-extending wings. As the plasma expands radially, it accumulates at the expanding front while a density depression progressively forms on axis ($0.3 \lesssim t \lesssim 2.7$ ns). At $t \sim 2.7 - 5.2$ ns the density gradient at the plasma front has steepened, and a shock front with a radiative precursor (indicated by the arrow in Fig. 2 (c)) has formed. As the shock propagates radially, its amplitude initially increases, eventually reaching a maximum at $t \sim 5.2$ ns, and subsequently decreases with a width increase.

To gain insight into the physical processes determining the evolution of the plasma, simulations were performed with the hydrodynamic code DUED[32] running in one-dimensional cylindrical geometry. DUED is a two-temperature Lagrangian fluid code including flux-limited multigroup radiation diffusion. The radiation package is run with 33 fixed energy photon groups and the relevant Argon opacities, the energy groups are distributed to account for temperature lowering. (The non-dynamical group re-distribution can be source of some uncertainty.) Opacities are provided by the SNOP code[33]. Electron thermal conduction is either treated with a flux-limited model or a nonlocal model[22,25]. In our simulations energy deposition by the laser pulse was modeled by imposing an initial spatial temperature distribution over a uniform density Argon background gas. The background gas density was taken equal to the experimentally measured value of $\sim 10^{18}$ cm^{-3}. An initial Gaussian temperature profile with a 1 keV peak temperature and a full-width half-maximum of 235 µm was chosen in such a way to best reproduce the radial plasma density profile at the earliest available experimental probing time, with the additional condition that total energy initially stored in the system equals the laser absorbed energy. Given these constraints, the initial parameters for the simulation were rather univocally determined. The employed setup creates a relatively hot plasma with pronounced thermal gradients, which readily reduce under the effect of nonlocal electron transport[16]. Simulations show that nonlocal transport effects influence the thermal wave evolution for a time interval of no more than 200 ps (see the red box in Fig. 4). Once the gradients smooth out, an

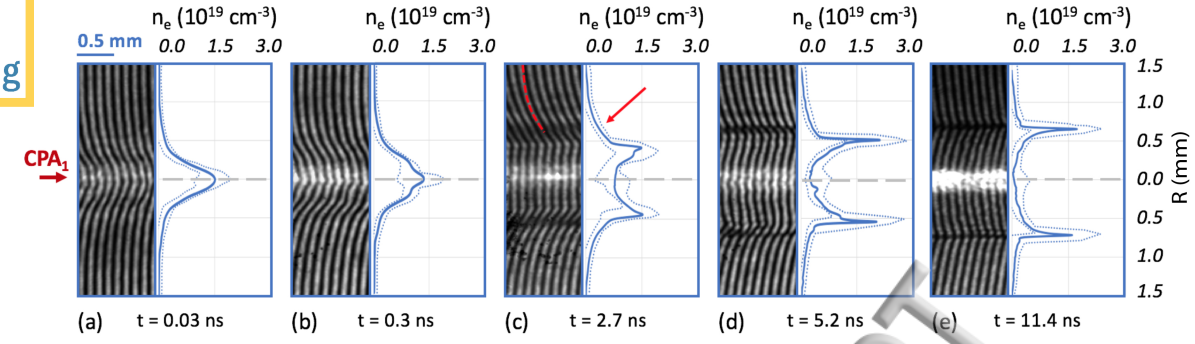

FIG. 2. Interferograms at different probing times and corresponding Abel-inverted electron density radial profiles in solid blue. Error bar margins are plot with blue dashed lines. The dashed line and the arrow in (c) indicate the radiative precursor.

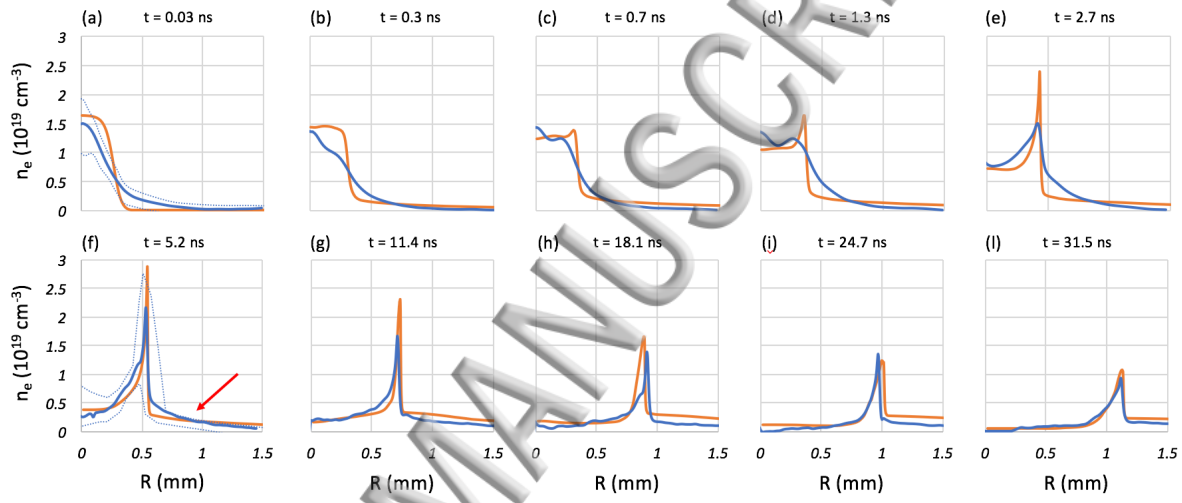

FIG. 3. Experimental (blue) and simulated (orange) electron density profiles at different times. In (a) and in (f) error bar margins are plotted with blue dashed lines. The arrow in (f) indicates the radiative precursor.

electron thermal wave is formed. The energy, still stored mostly in the electrons, is partly converted into ion kinetic energy seeding the shock formation. This phase spans from 0.3 to 5.2 ns [see frames (c)–(f) Fig. 3 and the blue shaded area in Fig. 4]. During this stage, the evolution of the shock-front radius is fitted by the power law $R \propto t^{0.22}$. When the rarefaction wave reaches the shock front (Fig. 3 (f)) a BW is launched [Fig. 3 (g)–(l)]. From this time on, the BW evolves in a radiative phase and the thin shell continuously radiates energy received from the hot remnant[11]. The radiative BW trajectory is fitted by the power law $R \propto t^{0.41}$. Figure 4 also shows the adiabatic and fully radiative snowplough cases for comparison. The effect of nonlocal heat conduction is the fast removal of energy from the hot filament, due to the the long-range electrons. As a consequence the electron-ion energy exchange is less efficient and the shock formation is delayed. Eventually, a heat conduction flux-limiter technique constraints the energy over a smaller volume seeding the almost immediate shock formation, (Fig. 5, Fig. 6). The effects of the removal of energy by radiation are also visible during the self similar phase as a reduced shock front velocity. At early times ($t \lesssim 2.7$ ns) the plasma front exhibits a weaker density gradient than the simulations [Fig. 3 (a)–(e)], as well as wings, probably due do hard-photon preheating, that are not reproduced by simulations. However, the front position at different times is approximately well described by the simulation at all times (Fig. 4). To best match the early time profiles the use of the nonlocal model is necessary, as shown in Fig. 5 and Fig. 6. From Fig. 5 a)-b). When the BW has fully formed, quantitative agreement is found between the simulation and the experiment both in terms of shock amplitude and shock front trajectory (Fig. 3 (f-l) and Fig. 4). Consistently with the experimental findings, a density precursor is observed in the simulations ahead of the shock front [see the arrow in Fig. 3 (f)]. A Sedov-Taylor scaling is also plotted for comparison in Fig. 4 (b), showing that the late-time BW trajectory is well reproduced by a power law $R \propto t^{\alpha}$ with a coefficient $\alpha \sim 0.41$. While a value of 0.5 is expected for an adiabatic cylindrical BW[19,20], a lower value for the exponent is a typical signature of radiative losses. Consistently, during this stage the observation of the density precursor can be attributed to preheating and ionization of the upstream gas by radiation emission from the thin shell. To address the question of the relative importance of the different physical processes at play, and to

distinguish the effects seeded by non local heat conduction at early and late times, DUED simulations with different models were carried out, i) including both radiation diffusion and nonlocal electron transport (Fig. 5) and with different flux-limiter values (Fig. 6), ii) with radiation off and nonlocal transport on, iii) with radiation on and the flux-limited model (with flux-limiter coefficient $f = 0.08$) and iv) with radiation off and flux-limiter on. The simulations indicate that at early times a major role is played by electron thermal conduction occurring in a nonlocal transport regime [simulations i) and ii), Fig. 5 (a)]. Indeed, in the early plasma expansion phase, nonlocal transport allows for energy spread on times shorter than the typical timescales for hydrodynamic expansion, ionizing the gas ahead of the plasma front and giving rise to a smooth radial density gradient. On the contrary, with the use of flux-limited conduction, thermal energy remains confined in a limited volume, causing the formation of a sharp density profile and triggering the generation of a shock wave already at early times. At later times, once the BW has formed, diffusive radiation losses become effective in reducing the BW propagation velocity and the shock amplitude in comparison to the non-radiative cases [Fig. 5 (b)]. Consistently these simulations confirm that radiative preheating and consequent ionization of the background gas are mainly responsible for the formation of the density precursor. In the case when the flux-limited model is used, the BW retains some memory of the early expansion phase, and even in the radiative case the shock front keeps its initial shift ahead of the experimentally observed shock front position [Fig. 5 (b)]. We also notice here that if a diffusive model with no flux-limiter is used, unrealistically fast BWs are obtained, which neither match the experimental density profiles nor the BW trajectory. In order to estimate the duration of the time intervals in which nonlocal transport and radiation effects respectively dominate, additional simulations were performed with the nonlocal transport package switched on in the early evolution phase, and later replaced by flux-limited modeling. Simulations performed in this configuration and with the inclusion of radiation diffusion resulted identical to the best-matching simulation [case i)] at all times whenever the nonlocal package is activated within the initial 0.2 ns. Later, at $t \approx (2.5 - 3)$ ns, simulations with radiation on or off begin to separate, showing that only after this time radiative cooling becomes effective.

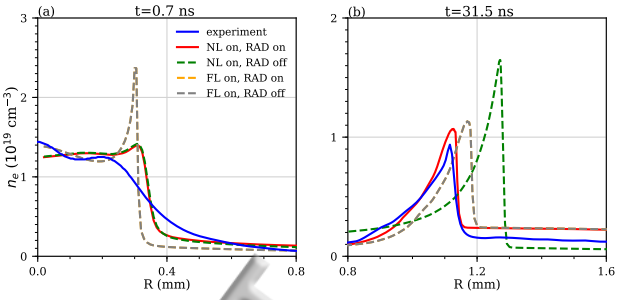

FIG. 5. Comparison of electron density profiles from experimental interferograms and DUED simulations for two selected times (a) $t = 0.7$ ns, (b) $t = 31.5$ ns and four different simulation conditions, i.e. with nonlocal transport (NL) or with a flux-limiter (FL), radiation (RAD) on and off.

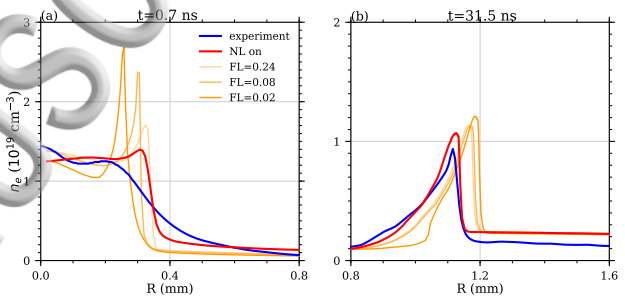

FIG. 6. Electron number density profiles at two selected times, for different flux-limiter values.

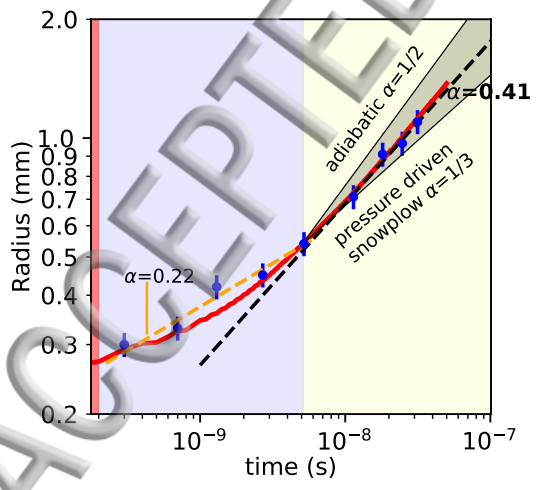

FIG. 4. Blast wave radius versus time: experimental data (blue dots) vs DUED simulations (solid red curve). A Sedov-Taylor power-law exponent $\alpha = 0.41$ is inferred for the radiative phase (yellow background), while $\alpha = 0.22$ is inferred for the thermal wave phase (blue background). The red background box highlights the time window where simulations predict nonlocal heat conduction major effects.

In conclusion, we characterized the full evolution of a cylindrical BW evolving from a laser-generated hot filament. The interaction of a short and intense laser pulse with an atomic cluster jet ensured appropriate conditions, namely, high (keV) plasma temperatures and steep thermal gradients, to investigate nonlocal electron transport and radiation diffusion. Detailed comparison of the experimental results with hydrodynamic simulations reveals that the plasma undergoes a transition from an initial expansion phase, dominated by nonlocal electron transport, to a BW propagation phase where radiative losses become non-negligible.

ACKNOWLEDGMENTS

The research has received funding from LASERLAB-EUROPE (grant 654148, European Union's Horizon 2020). A.M. acknowledges SILMI Exchange Grant, L.R. ULIMAC-GRANT Triangle de la Physique. SA was partly supported by Sapienza Grants C26A15YTMA, 2016-257584 and Eurofusion project AWP17-ENR-IFE-CEA-01, Y.F. and S.J. by Grant-in-Aids for Scientific Research (A) No. 26247100 by JSPS.

[1] S. Atzeni and J. Meyer-ter Vehn, *The Physics of Inertial Fusion: BeamPlasma Interaction, Hydrodynamics, Hot Dense Matter* (Oxford University Press, 2004).
[2] J. D. Lindl, P. Amendt, R. L. Berger, S. G. Glendinning, S. H. Glenzer, S. W. Haan, R. L. Kauffman, O. L. Landen, and L. J. Suter, Physics of Plasmas **11**, 339 (2004).
[3] R. S. Craxton, K. S. Anderson, T. R. Boehly, V. N. Goncharov, D. R. Harding, J. P. Knauer, R. L. McCrory, P. W. McKenty, D. D. Meyerhofer, J. F. Myatt, and et al., Physics of Plasmas **22**, 110501 (2015).
[4] R. P. Drake, *High-energy-density physics: fundamentals, inertial fusion, and experimental astrophysics* (Springer Science & Business Media, 2006).
[5] G. Gregori, A. Ravasio, C. D. Murphy, K. Schaar, A. Baird, A. R. Bell, A. Benuzzi-Mounaix, R. Bingham, C. Constantin, R. P. Drake, and et al., Nature **481**, 480 (2012).
[6] B. A. Remington, D. Arnett, R. Paul, and H. Takabe, Science **284**, 1488 (1999).
[7] A. S. Moore, J. Lazarus, M. Hohenberger, J. S. Robinson, E. T. Gumbrell, M. Dunne, and R. A. Smith, Astrophysics And Space Science **307**, 139 (2007).
[8] A. S. Moore, D. R. Symes, and R. A. Smith, Physics of Plasmas **12**, 2707 (2005).
[9] K. A. Keilty, E. P. Liang, T. Ditmire, B. A. Remington, K. Shigemori, and A. M. Rubenchik, The Astrophysical Journal **538**, 645 (2000).
[10] E. Liang and K. Keilty, The Astrophysical Journal **533**, 890 (2000).
[11] M. J. Edwards, A. J. MacKinnon, J. Zweiback, K. Shigemori, D. Ryutov, A. M. Rubenchik, K. A. Keilty, E. Liang, B. A. Remington, and T. Ditmire, Physical Review Letters **87**, 85004 (2001).
[12] A. D. Edens, T. Ditmire, J. F. Hansen, M. J. Edwards, R. G. Adams, P. Rambo, L. Ruggles, I. C. Smith, and J. L. Porter, Physics of Plasmas (1994-present) **11**, 4968 (2004).
[13] D. R. Symes, M. Hohenberger, J. Lazarus, J. Osterhoff, A. S. Moore, R. R. Fäustlin, A. D. Edens, H. W. Doyle, R. E. Carley, A. Marocchino, and et al., High Energy Density Physics **6**, 274 (2010).
[14] M. Hohenberger, D. R. Symes, J. Lazarus, H. W. Doyle, R. E. Carley, A. S. Moore, E. T. Gumbrell, M. M. Notley, R. J. Clarke, M. Dunne, and R. A. Smith, Physical Review Letters **105**, 205003 (2010).
[15] J. F. Hansen, M. J. Edwards, D. H. Froula, A. D. Edens, G. Gregori, and T. Ditmire, in *High Energy Density Laboratory Astrophysics* (Springer Netherlands, Dordrecht, 2007) pp. 219–225.
[16] T. Ditmire, E. T. Gumbrell, R. A. Smith, A. Djaoui, and M. Hutchinson, Physical Review Letters **80**, 720 (1998).
[17] A. S. Moore, E. T. Gumbrell, J. Lazarus, M. Hohenberger, J. S. Robinson, R. A. Smith, T. J. A. Plant, D. R. Symes, and M. Dunne, Physical Review Letters **100**, 055001 (2008).
[18] R. A. Smith, J. Lazarus, M. Hohenberger, A. Marocchino, J. S. Robinson, J. P. Chittenden, A. S. Moore, E. T. Gumbrell, and M. Dunne, Plasma Physics and Controlled Fusion **49**, B117 (2007).
[19] L. I. Sedov, *Similarity and Dimensional Methods in Mechanics, New York: Academic Press* (1959).
[20] Y. B. Zeldovich and Y. P. Raizer, *Physics of shock waves and high-temperature hydrodynamic phenomena*, Tech. Rep. (Academic Press, New York, 1966).
[21] J. Luciani, P. Mora, and J. Virmont, Physical Review Letters **51**, 1664 (1983).
[22] G. P. Schurtz, P. D. Nicolai, and M. Busquet, Physics of Plasmas (1994-present) **7**, 032701 (2000).
[23] P. D. Nicolai, J. Feugeas, and G. P. Schurtz, Physics of Plasmas (1994-present) **13**, 4238 (2006).
[24] W. Manheimer, D. Colombant, and V. Goncharov, Physics of Plasmas **15**, 083103 (2008).
[25] A. Marocchino, M. Tzoufras, S. Atzeni, A. Schiavi, P. D. Nicolaï, J. Mallet, V. Tikhonchuk, and J.-L. Feugeas, Physics of Plasmas **20**, 022702 (2013).
[26] D. Del Sorbo, J. L. Feugeas, P. Nicolai, M. Olazabal-Loume, B. Dubroca, S. Guisset, M. Touati, and V. Tikhonchuk, Physics of Plasmas (1994-present) **22**, 082706 (2015).
[27] L. Spitzer and R. Härm, Physical Review **89**, 977 (1953).
[28] R. C. Malone, R. L. McCrory, and R. L. Morse, Physical Review Letters **34**, 721 (1975).
[29] R. P. Drake, J. J. Carroll, T. B. Smith, P. Keiter, S. G. Glendinning, O. Hurricane, K. Estabrook, D. D. Ryutov, B. A. Remington, R. J. Wallace, E. Michael, and R. McCray, Physics of Plasmas **7**, 2142 (2000).
[30] G. Schurtz, S. Gary, S. Hulin, C. Chenais-Popovics, J. C. Gauthier, F. Thais, J. Breil, F. Durut, J. L. Feugeas, P. H. Maire, and et al., Physical Review Letters **98** (2007).
[31] T. Ditmire, K. Shigemori, B. A. Remington, K. Estabrook, and R. A. Smith, Astrophysical Journal Supplement Series **127**, 299 (2000).
[32] S. Atzeni, A. Schiavi, F. Califano, F. Cattani, F. Cornolti, D. Del Sarto, T. V. Liseykina, A. Macchi, and F. Pegoraro, Computer Physics Communications **169**, 153 (2005).
[33] K. Eidmann, Laser and Particle Beams **12**, 223 (1994).

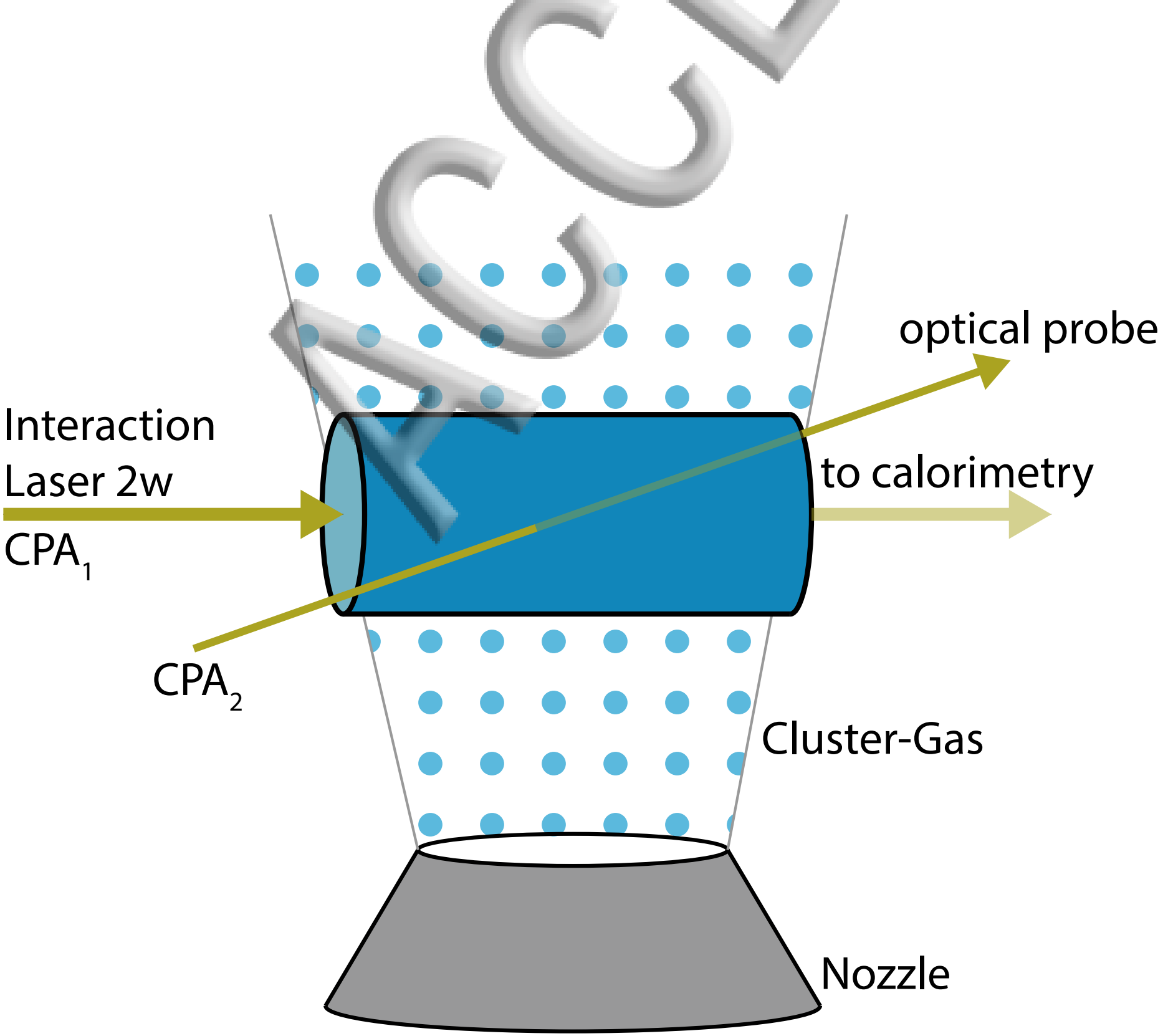
optical probe
Interaction
Laser 2w
CPA1
to calorimetry
CPA2
Cluster-Gas
Nozzle

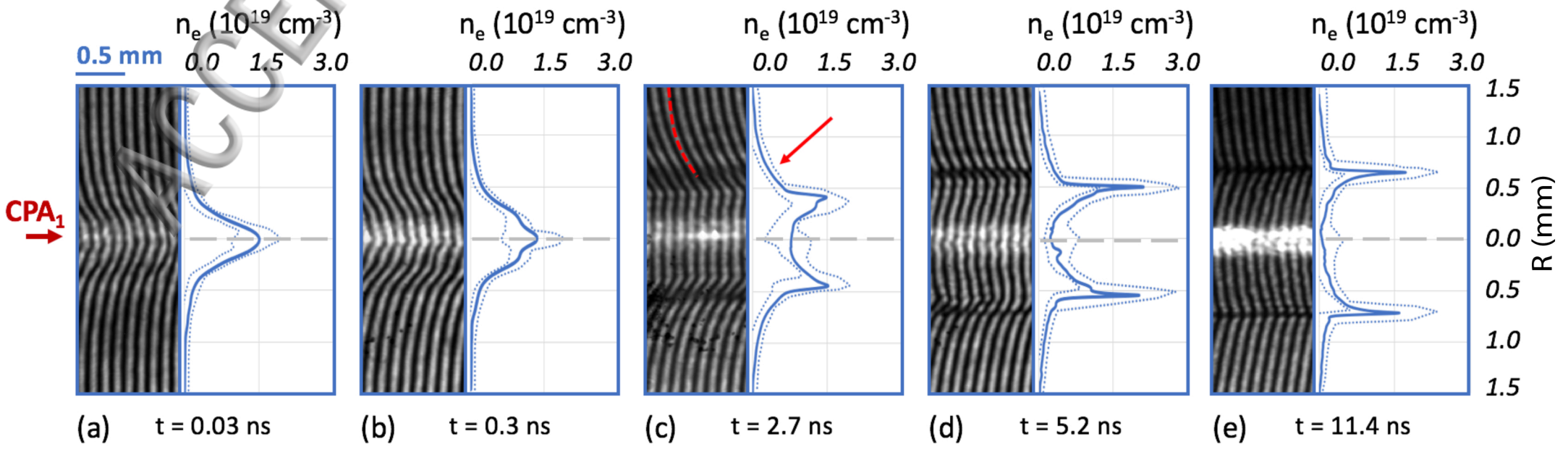
n_e (10^{19} cm^{-3})
0.0 1.5 3.0
0.5 mm
CPA$_1$
R (mm)
1.5 1.0 0.5 0.0 0.5 1.0 1.5
(a) t = 0.03 ns
(b) t = 0.3 ns
(c) t = 2.7 ns
(d) t = 5.2 ns
(e) t = 11.4 ns

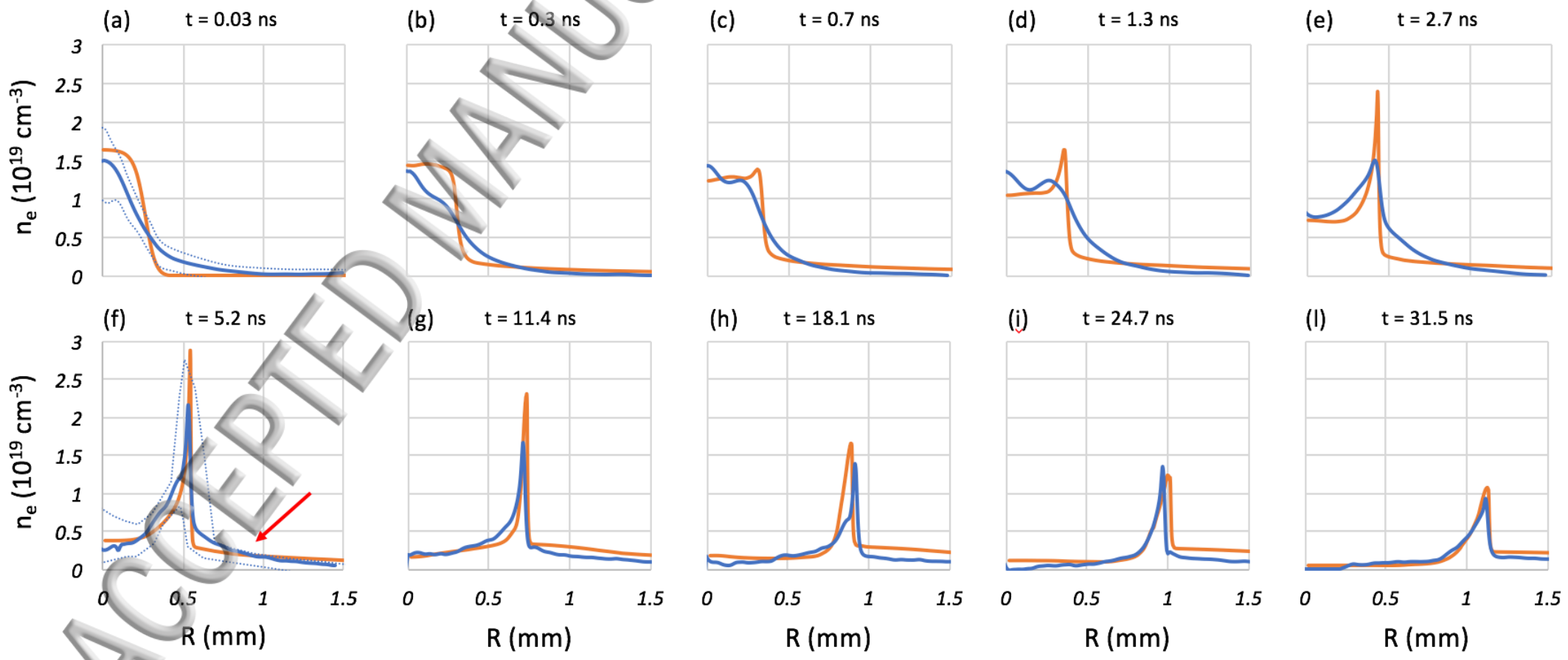

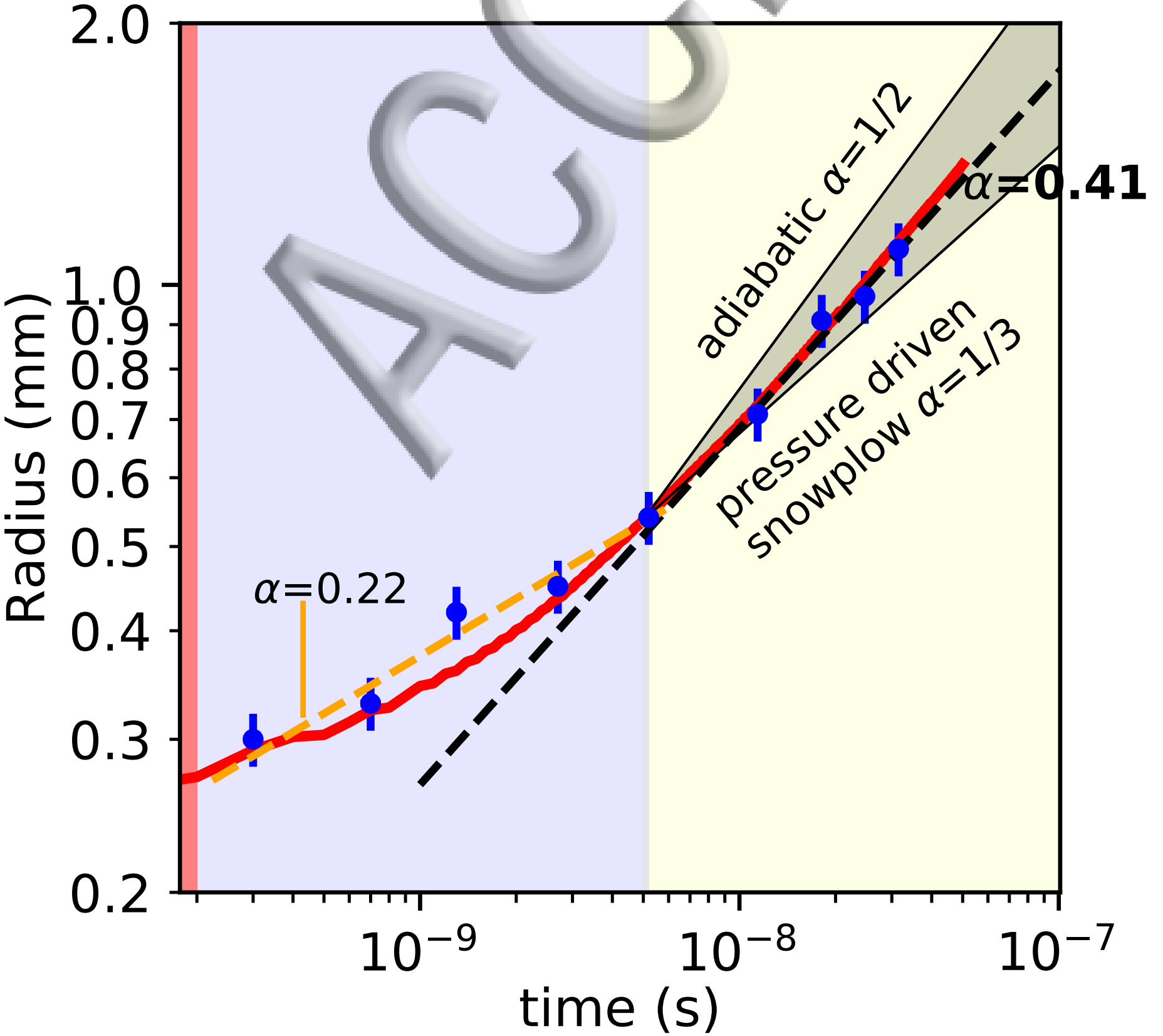
2.0
1.0
0.9
0.8
0.7
0.6
0.5
0.4
0.3
0.2
Radius (mm)
10^{-9}
10^{-8}
10^{-7}
time (s)
adiabatic α=1/2
α=0.41
pressure driven
snowplow α=1/3
α=0.22

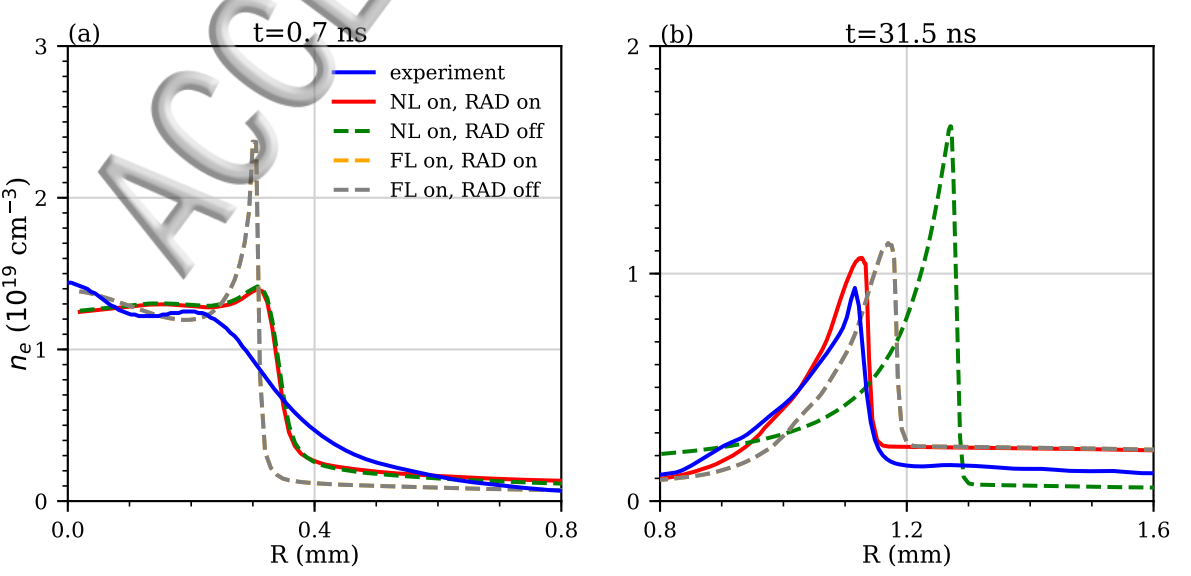
(a)
t=0.7 ns
experiment
NL on, RAD on
NL on, RAD off
FL on, RAD on
FL on, RAD off
n_e (10^{19} cm^{-3})
R (mm)
(b)
t=31.5 ns
R (mm)

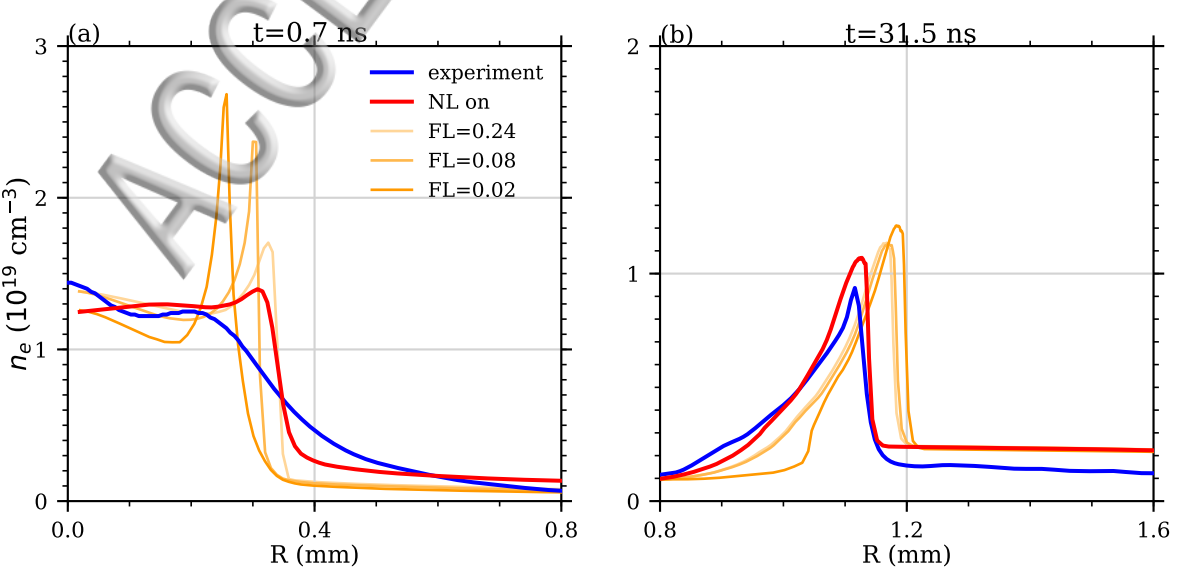
(a)
t=0.7 ns
experiment
NL on
FL=0.24
FL=0.08
FL=0.02
n_e (10^{19} cm^{-3})
R (mm)
(b)
t=31.5 ns
R (mm)